Advances in Science and Technology Research Journal

Advances in Science and Technology Research Journal, 2026, 20(10), 237–249
https://doi.org/10.12913/22998624/225093
ISSN 2299-8624, License CC-BY 4.0

Received: 2026.05.27
Accepted: 2026.07.26
Published: 2026.09.01

Investigation of failure causes in a modern single-axis solar tracker structure

Piotr Woźniczka[1*], Paulina Zajdel[1], Grażyna Gaszyńska-Freiwald[1], Karol Kołat[1]

[1] Faculty of Civil Engineering, Cracow University of Technology, Warszawska 24, 31-155 Krakow, Poland
* Corresponding author's e-mail: piotr.wozniczka@pk.edu.pl

ABSTRACT

The paper presents a recent failure that occurred during the construction phase of a utility-scale photovoltaic power plant with a total capacity exceeding 20 MW. Modern single-axis tracker structures and PV modules were damaged during a severe summer storm. The study includes an analysis of the construction work carried out on site, as well as an assessment of the available design documentation. To verify the correctness of the applied structural solutions, numerical models of the investigated system were developed. A frequency analysis and an assessment of possible torsional galloping occurrence were performed. Based on the conducted investigations, it was concluded that the failure resulted from a combination of factors, including incorrect assumptions regarding design loads, design and execution errors, and excessive simplifications adopted in the structural modelling process. Complex soil conditions at the construction site were also found to be a significant contributing factor. The conducted analysis indicated that the requirements of current standards were not satisfied with respect to both ultimate and serviceability limit states. Consequently, structural strengthening measures were proposed. Introduction of additional bracings, foundations and dampers enabled compliance with the current standards requirements.

Keywords: steel structures, failure analysis, photovoltaic systems, PV panels, single-axis tracker, solar tracker

INTRODUCTION

The global shift away from fossil fuels has significantly intensified interest in renewable energy sources, particularly photovoltaic (PV) systems. Current projections indicate [1] that in the coming years a further increase of more than 37% in the installed photovoltaic systems capacity is expected. Consequently, the total installed capacity is forecast to exceed 1580 GW by 2030. Simultaneously, in most cases [1], the energy produced using photovoltaic panels is economically competitive with energy generated from conventional fossil-fuel technologies. New mounting techniques have been proposed [2], and among the innovative solutions enabling further improvements in the performance and efficiency of photovoltaic installations are single-axis (referred to hereafter as SATS) and dual-axis (referred to hereafter as DATS) solar tracking systems [3]. In both configurations, the structure allows for rotation and adjustment of panel orientation relative to the sun's path. For DATS systems, which enable movement in both the north–south and east–west directions, the increase in energy yield relative to traditional fixed-tilt installations can reach up to 45%. It must be noted, however, that DATS systems are characterized by considerable structural complexity, which consequently results in higher installation costs. In this context, the simpler SATS systems, which allow panel rotation only in the east–west direction, have gained increasing interest. A complete SATS structure, including technical specifications, is presented in [4]. That study also provides measurement results demonstrating that the use of a SATS solution yields an approximately 30% increase in energy production compared to conventional fixed-tilt installations.

The introduction of these innovative tracking mechanisms has necessitated comprehensive investigations into the structural behavior of such systems. In [5], full-scale experimental tests are reported, including measurements of wind velocity, natural frequencies, and the determination of pressure coefficients for SATS structures. It was shown that the pressure coefficients recommended for fixed panels in ASCE 7-22 [6] are conservative compared to the experimentally obtained values. The authors of [5] also emphasized the need for more detailed research on the fatigue resistance of PV-supporting structures. Complementary results from wind-tunnel investigations and computational fluid dynamics (CFD) simulations are presented in [7]. Analyses crucial to ensuring the structural safety of solar trackers under dynamic wind loads are discussed in [8], [9], and [10]. Issues related to the foundation design for photovoltaic farms are reviewed in [11].

Despite these research efforts and technological developments, several failures of PV support structures have occurred in recent years. In multiple cases involving SATS structures ([12], [13], [14]), wind-induced dynamic effects were identified as the primary cause of structural damage. Significant failures of non-tracking systems have been attributed to incorrect estimation of wind loads and errors in steel design procedures [15]. In the case described in [16], the direct cause of the structure's destruction was the use of an unconventional and unverified connection detail. A comprehensive discussion of the impact of various human errors on the design and execution of steel structures is described in [17].

In this context, the present article analyses a recent failure that occurred during the construction of a utility-scale PV power plant with a total capacity exceeding 20 MW. Damage to a modern SATS-type tracking system resulted from a combination of several contributing factors. A review of project documentation revealed inappropriate load assumptions, design errors, and excessive simplifications in structural modelling. Complex soil conditions at the construction site were also found to be a significant contributing factor. The article presents an assessment of the investigated solar-tracker structure and outlines potential strengthening measures, although their implementation proved difficult due to the scale of the installation.

EXPERIMENT

Description of the solar-tracker structure

The photovoltaic farm was constructed on a flat, sparsely developed site. The width of the farm in the north–south direction reached nearly 1000 m. The photovoltaic panels were mounted on irregularly spaced SATS-type structures. The subsequent rows were arranged at an axial spacing of 5 m; however, they were mutually shifted and differed in length. The structure enabled rotation of the panels in the east–west direction within a range of ±60°, and as a result, a minimum clearance of 2.5 m remained between the panels of adjacent rows.

The maximum length of a single SATS structure was 69 m. Standard columns were made of individually designed cold-formed channels with a height of 105 mm, flange width of 50 mm and a thickness of 3 mm. These columns were spaced at a maximum distance of 5300 mm. A motor-support column made of a built-up, cold-formed I-section was installed at the mid-length of each structure. A longitudinal purlin made of SHS 100×3 was placed on the columns, and appropriate bearings were introduced to enable rotation. It should be noted that the use of SHS is a common solution, with similar sections applied in [4] and [12]. Panels with dimensions of 1303 × 2384 mm were mounted to the purlin using profiles with dimensions 52 × 99 mm. These profiles were additionally reinforced in the vicinity of the purlin. All components were manufactured from standard structural steel S350 GD. At each end of the structure, a damper was mounted. In the event of a sudden increase in load, these dampers were intended to lock the rotation of the purlin. The maximum load capacity of a single damper was 17 kN. The C-section columns were driven directly into the soil to a depth ranging from 1500 to 2000 mm. The embedment depth was determined based on field tests involving pull-out tests and measurements of horizontal displacements under loading. However, no direct measurement of driving force was performed during pile installation. Selected structural details of the tracker are presented in Figure 1.

The structure was also equipped with an electronic system designed to prevent damage caused by excessive wind or snow loading. When wind speed exceeded 14 m/s, the panels automatically rotated to a safe position (panel tilt angle of 5°).

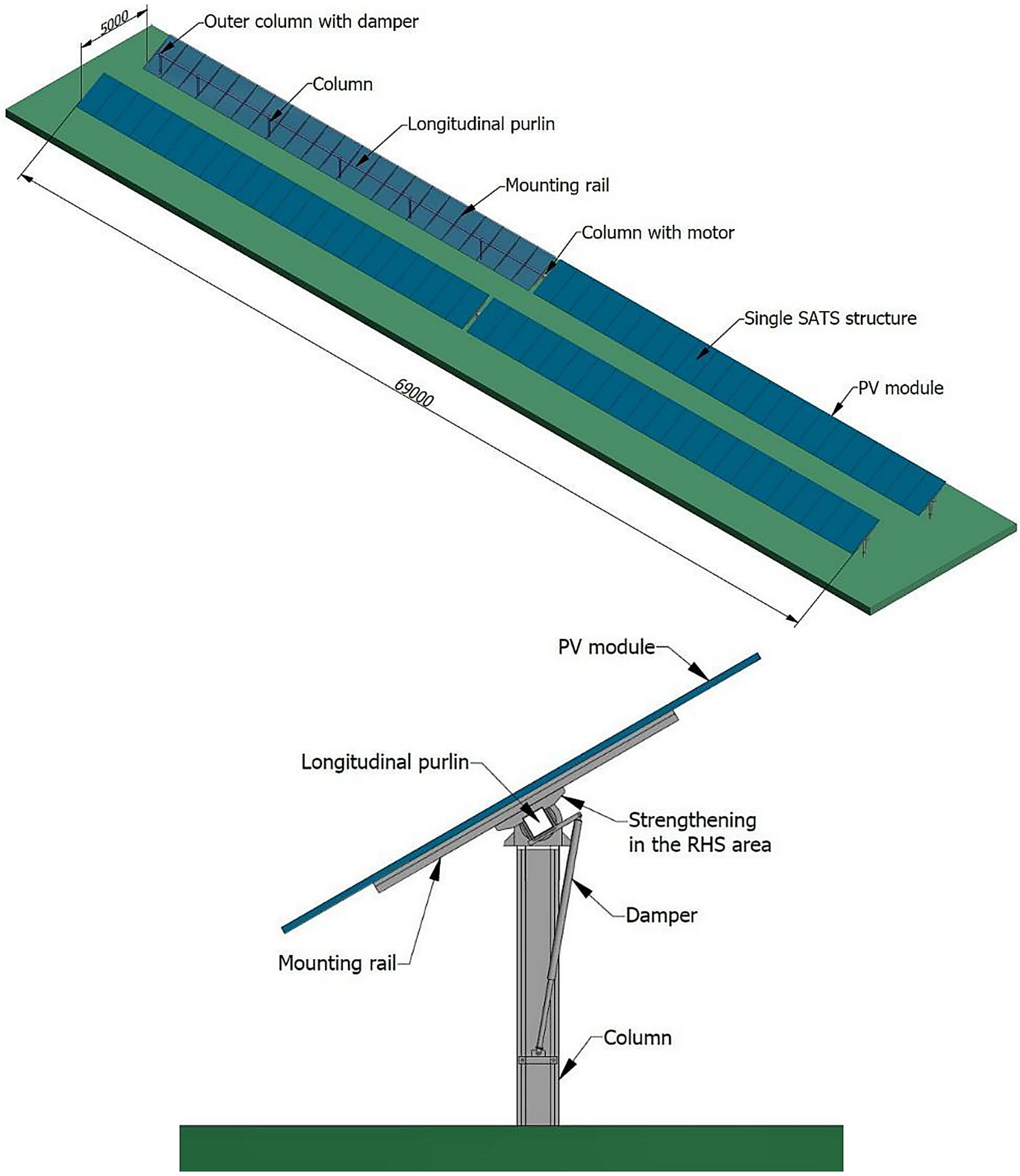

Figure 1. Solar-tracker structure: a) general view of two consecutive structures b) side view

The rotation time from 60° to 5° was approximately 6 minutes. When snow load exceeded 0.20 kN/m², the panels rotated to the 60° position, causing the snow to slide off the panels.

Failure of the structure

The support structure was damaged in summer during a storm, with wind gusts reaching speeds of up to 23 m/s. At the time of the failure, the structure was not complete and was still in the assembly phase. The most critical issues were the absence of the end dampers and the lack of an electrical connection, which prevented the proper operation of the automatic protection systems described above. Additionally, significant amounts of water accumulated in terrain depressions in the vicinity of the columns. Available industrial-camera recordings indicate that torsional galloping occurred in at least some of the support structures. The damage observed after the storm included, among others, panel surface wrinkling, bearing failures, and permanent deformation of the columns (Figure 2).

Analysis of the project documentation

After the failure occurred, it was not clear whether the damage was caused solely by the current state of the structure during the assembly

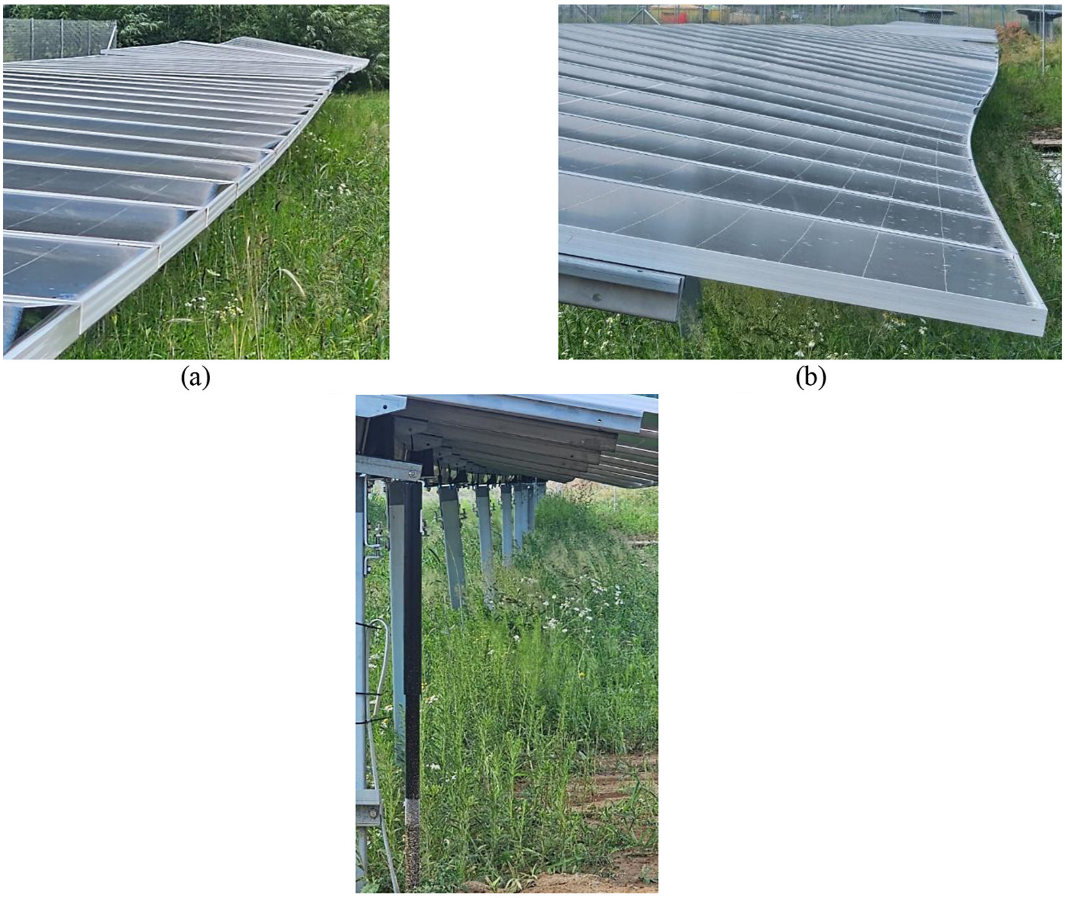

(a) (b) (c)

Figure 2. Selected structural damages: a) and b) wrinkling of the photovoltaic panel surfaces c) permanent displacements of the columns

phase or whether similar failures could potentially recur after the completion of construction. In this situation, it was decided to perform an analysis of the available project documentation.

The structural design had been prepared by licensed engineers. The structure was classified as consequence class CC1 (minor economic consequences of failure) and reliability class RC1 in accordance with the provisions of standard [18]. The adopted assumptions resulted in a reduction of the design loads by 10% compared to the values typically applied for class RC2. Taking into account the scale of the installation and the economic consequences of its potential shutdown, the authors consider that it would be more appropriate to adopt classes CC2 and RC2.

Permanent loads and snow load were specified correctly in the project. Wind load was determined using standard [19]. The wind-speed values were reduced based on a design working life of 25 years for the structure. It should be noted that standard [19] does not contain detailed guidelines regarding wind loading of photovoltaic panels. In this situation, the loads were calculated analogously to single-slope roofs with inclination angles of 5° and 30°. As part of further simplifications, for the 60° position, the load coefficients corresponding to a 30° inclination angle were adopted. However, in the load tables prepared in the design documentation, only uniformly distributed surface loads determined on the basis of net pressure coefficients [19] were included. The case of non-uniform loading of the structure (global force coefficients according to [19]) was entirely omitted. A comparison of the loading scheme applied in the design and the correct wind-load scheme is presented in Figure 3.

Further issues identified in the design concerned primarily the manner in which the computational model had been prepared and its lack of compliance with the actual construction method. First, the computer model did not take into account the eccentric position of the panels with respect to the axis of the SHS 100×3 purlin. The cantilevered parts of the panels extending beyond

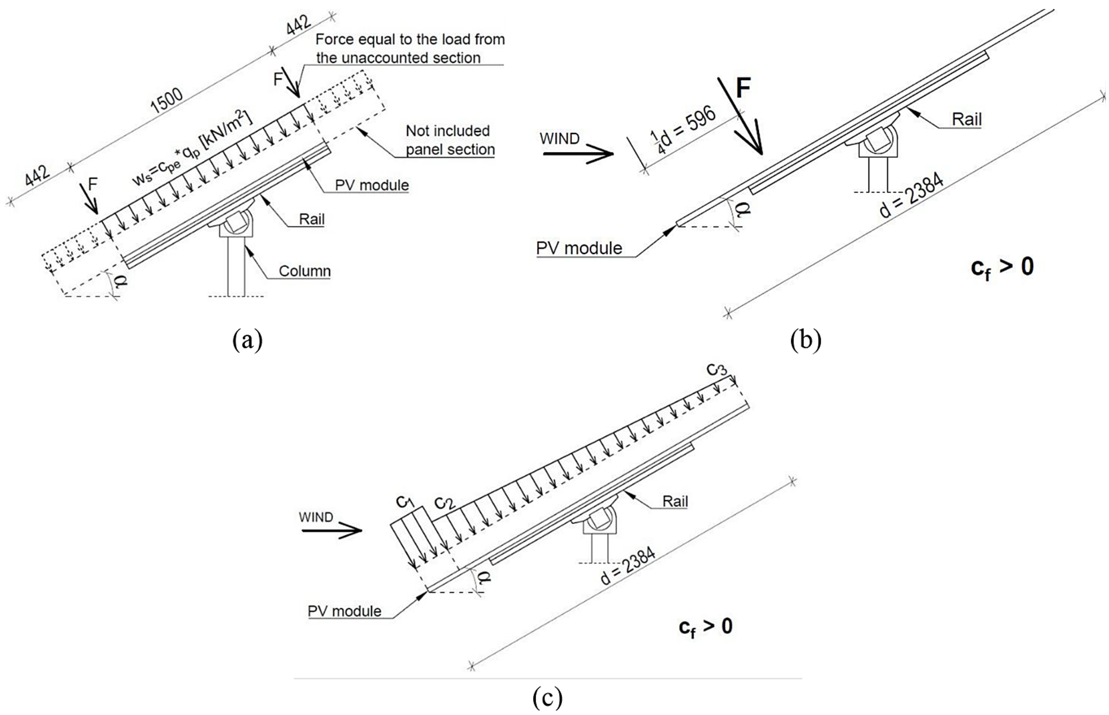

Figure 3. Wind-load scheme: a) scheme adopted in the design b) correct scheme according to standard [19] c) correct scheme according to guideline [20]. Only wind-pressure case is shown (without the wind-suction case)

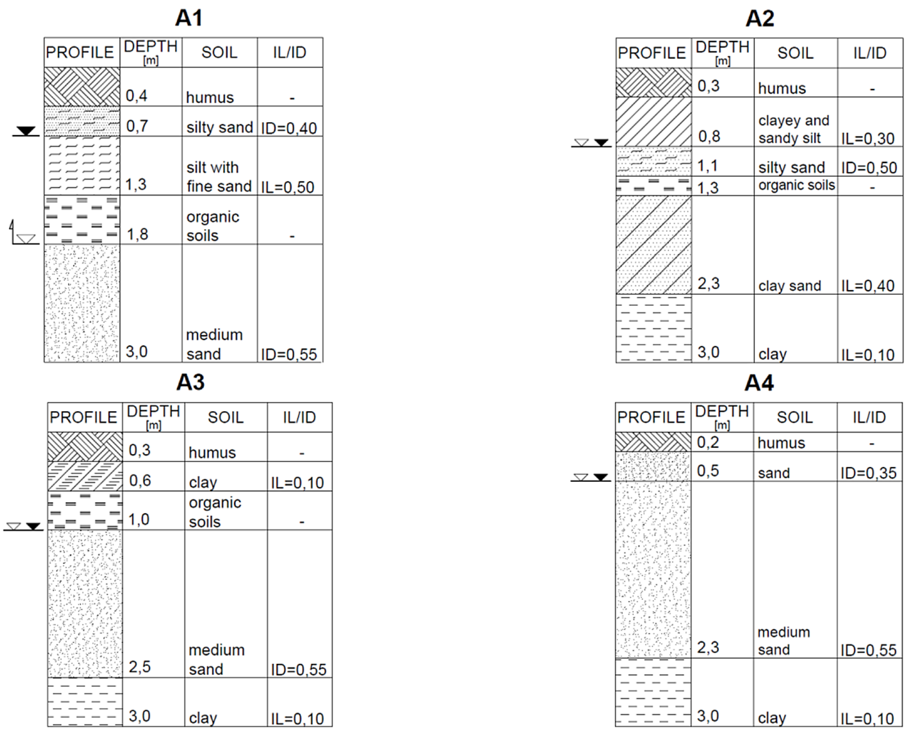

Figure 4. Selected geological data (A1–A4)

the rails were also omitted, which led to a further reduction in the wind-load eccentricity.

Another highly significant detail was the manner in which the structural support was modelled. In the design, fixed support was assumed at a level 0.30 m below ground level. In reality, the stiffness of the column embedment in the soil was very low, which was a direct result of the assumptions adopted during the field tests. The test columns were driven to a depth of 1500 mm and then loaded with a force corresponding to the characteristic horizontal reaction. Simultaneously, horizontal displacements at ground level were measured. The embedment depth was considered adequate when the displacement measured in this manner did not exceed 20 mm. When this condition was not met, the embedment depth was increased and the procedure was repeated. As a result, embedment depths ranging from 1500 to 2000 mm were applied on site. Nevertheless, regardless of the final embedment depth, each column was able to displace at ground level by up to 20 mm, which in no way corresponded to the fixed support model used in the calculations. The significant displacements were caused by the low stiffness parameters of the soil (plastic soils). Selected geological data are depicted in Figure 4 to present the variability of the ground conditions across the area of the photovoltaic farm. In many locations layers similar to those identified in borehole A4 were identified. However, at the same time layers like for cases A1–A3 were observed at nearby measurement points. A high groundwater level was also observed at all investigated locations. A schematic comparison of the structural model applied in the design and a more detailed and accurate model is presented in Figure 5.

In the project, no results of natural frequency analysis or the dynamic response analysis of the structure were presented. There was also no information regarding any potential method for modelling the damper. The scope of the geotechnical investigation raised additional doubts. Site investigation boreholes were executed at 70 m spacing. Such a large spacing did not allow for a precise determination of soil conditions, which were characterized by significant variability. According to national regulations, the soil conditions had to be classified as complex (plastic soils, high groundwater level, locally occurring organic peat soils). However, the project did not specify the method by which the soil parameters were determined. The tracker manual also stated that the structure may fail at a wind speed of 22 m/s. This value corresponds to the basic wind speed for the wind zone in which the photovoltaic farm is located. Nevertheless, it is not a value that can be directly applied in calculations intended to demonstrate the potential failure of the structure.

COMPUTER MODELING AND ANALYSIS

Considering the doubts described above regarding the correctness of the design documentation for the analyzed structure, appropriate computational models were developed using AxisVM X8 software [21]. The structure was modelled using standard beam elements. The dampers were included as spring-type elements with a rigid–plastic force–displacement characteristic. The

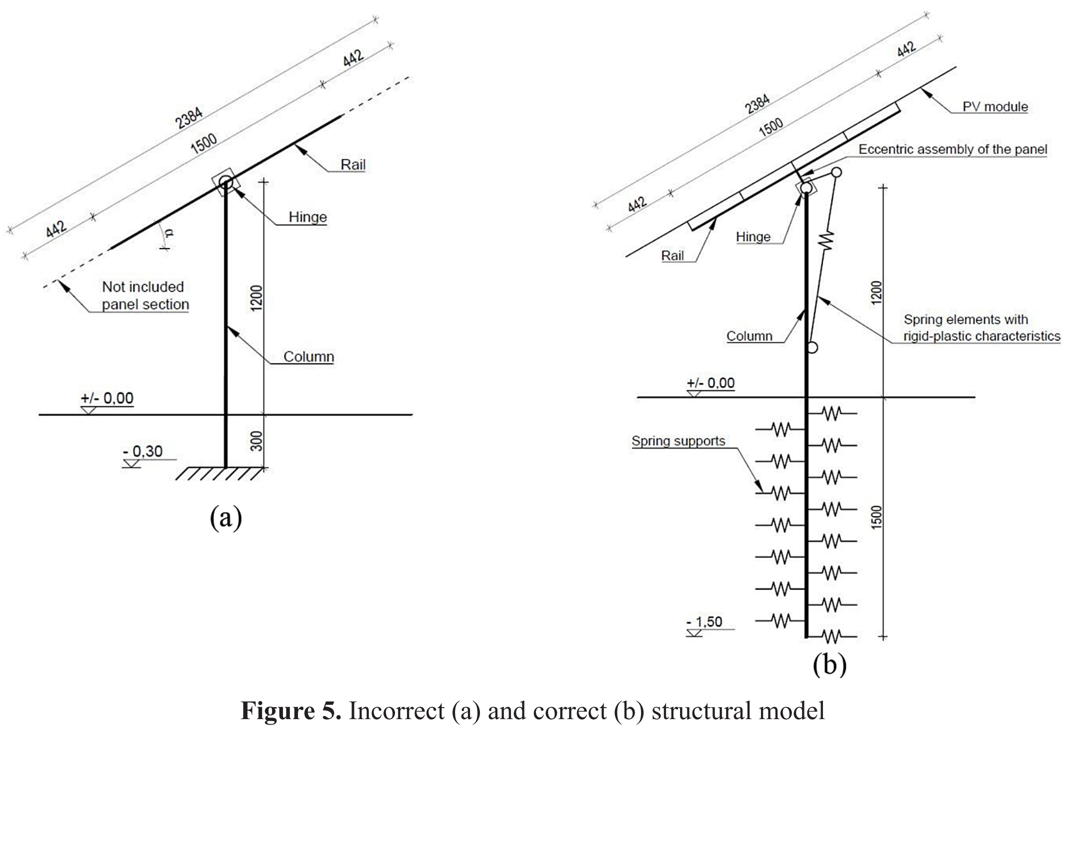

Figure 5. Incorrect (a) and correct (b) structural model

ultimate capacity of the element was set at 17 kN. In order to improve convergence, minimal material stiffening was introduced (a force of 17.1 kN corresponding to a deformation of 100 mm). With regard to wind loading, the application of standards [6], [19] and [22] was considered. Ultimately, due to the location of the photovoltaic farm, the wind load was determined in accordance with French national supplement [20] to [19], which constitutes a clarification of the provisions of [19]. For comparison purposes, withdrawn Polish standard [22] was also used. Its application was justified as it was used as a reference standard by the designer. The supports of the structure were modelled in two ways. In the first variant, fixed supports were assumed analogously to the original design. This was intended to enable further comparisons. In the second variant, the soil layers were modelled using Winkler springs. The horizontal stiffness of each spring was determined based on calculations carried out in accordance with general method described in [23]. Site-specific geological data were taken into account. In the next step obtained displacements of the columns were compared with measurements carried out during pile (column) installation works. As a result a convergence level of 90% was achieved. Thus, for example, for a selected column the measured displacement was 20 mm, while the corresponding FE modelling value was 18 mm. The results should be considered as conservative as they slightly underestimate the actual displacements of the structure. The design of the elements was performed in accordance with standards [24]

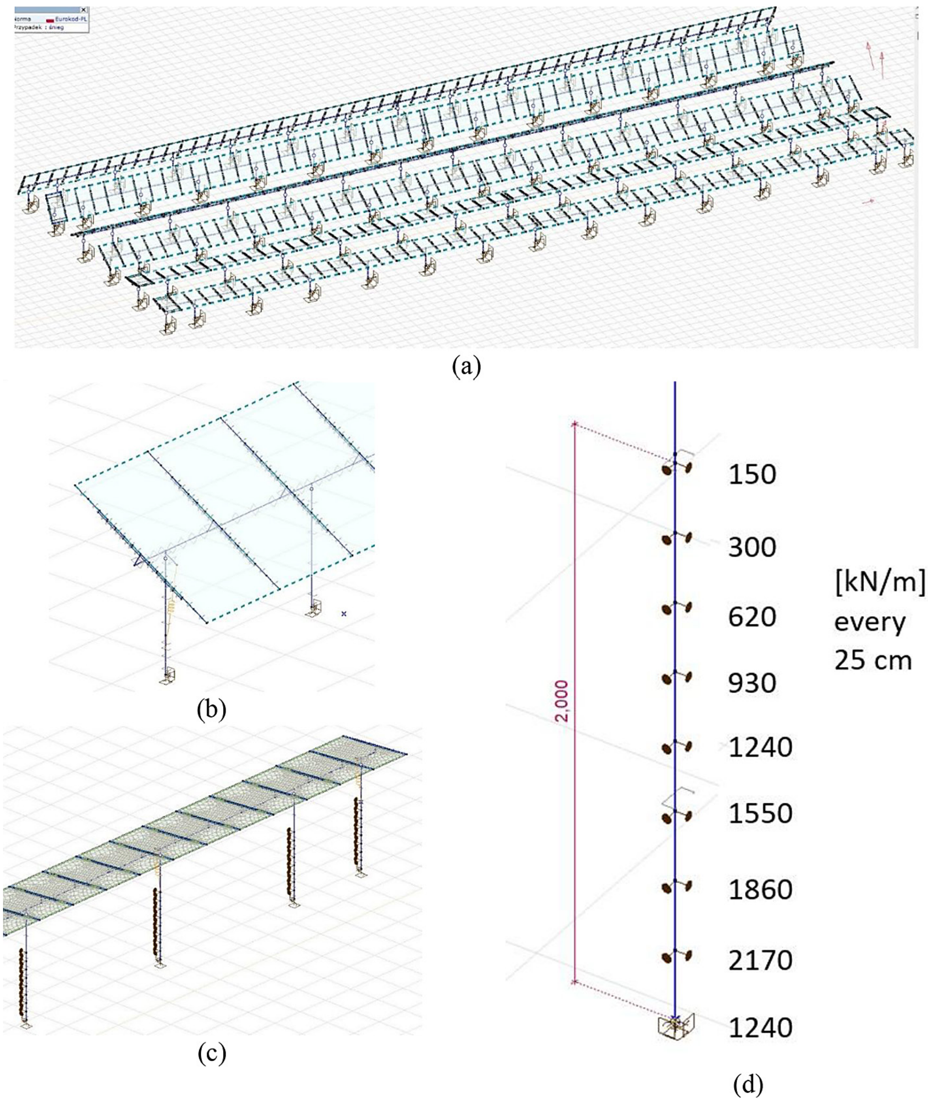

Figure 6. Details of the applied computational model: a) models for various angles of PV panels, b) detail of the end section of the structures, c) model with elastic supports and panels modelled using shell elements, d) values of spring stiffness

and [25]. Buckling modes of cold-formed members were determined using separate shell models. In the case of the natural frequency analysis, the panels were modelled using shell elements with a thickness of 35 mm. Variant analyses were performed for Young's modulus values ranging from 70 GPa to 165 GPa and with a Poisson's ratio equal to 0.22 [26]. Verification calculations were also carried out for the state of the structure at the moment of failure, i.e. with the dampers not installed. Selected details of the computational model are shown in Figure 6.

RESULTS AND DISCUSSION

In Tables 1 and 2, selected calculation results are presented. Only those cases involving elements that did not meet the relevant code requirements ([24], [25]) or that raised doubts regarding their impact on the structural behavior were included. All code checks were performed using [21].

As follows from the compiled data, irrespective of the method used to determine the wind load, the ultimate limit state conditions were not satisfied for the columns and for the longitudinal purlin. In the case of the purlin, the elastic torsional capacity of the cross-section was not satisfied. In turn, for the columns, the stability condition of the members was not met. At the same time, the cross-section utilization ratio corresponded to its full plastic resistance. Exceeding the code requirements should not occur. However, it must be acknowledged that the exceedances were not extremely large and would probably not directly cause the failure of the structure.

A much more significant issue was indicated by the calculated values of displacements and rotations. As already mentioned, the full wind load was considered only for the 5° position. For the remaining inclination angles, the load corresponding to a wind speed of 14 m/s was assumed, which resulted from the applied protection systems. Due to its flexibility the structure was not capable of maintaining the safe 5° position under wind loading. As a consequence, the panels could be subjected to the full wind load at an inclination angle reaching even 40°, which clearly results in a substantial increase in the applied loads. A comparison of loads acting on the structure for inclinations of 5° and 40° is presented in Figure 7. It should be noted that the presented loads are based on standard recommendations. Therefore, susceptibility to dynamic actions is not directly taken into account. Moreover, it was observed that in the state of the structure at the time of failure (without the dampers), the purlin rotation angle was even greater than that presented in Table 2 and reached up to 61°.

Table 1. Selected results in the ultimate limit state

Element	Condition	Wind load according to [20]	Wind load according to [22]	Comments
SHS purlin	$\frac{\tau_{Ed}}{f_y/\sqrt{3}\gamma_{M0}}$	144 %	128%	Condition not satisfied for panels at the position of 5º
C-section column	$\frac{M_{Ed}}{\chi_{LT}W_y f_y/\gamma_{M0}}$	130 %	115%	Condition not satisfied for panels at the position of 60º

Note: Governing load combination 0.9·1.15·G + 0.9·1.50·W, where G – dead load, W – wind load.

Table 2. Selected results for the serviceability limit state

Element	Condition	Wind load according to [20]	Wind load according to [22]	Comments
SHS purlin	Purlin rotation angle	36°	31º	Significant deformation for panels at the position of 5º
C-section column (support model)	Horizontal displacement at the top of the columns – according to [24] max. 10 mm, according to manufacturer max. 30 mm due to technological reasons	25 mm	25 mm	Condition not satisfied for panels at the position of 60º, computational model with fixed supports
Channel section column (soil-flexibility model)		81 mm	---	Condition not satisfied for panels at the position of 60º, soil modelled using spring supports

Note: Governing load combination 1.0·G + 1.0·W, where G – dead load, W – wind load.

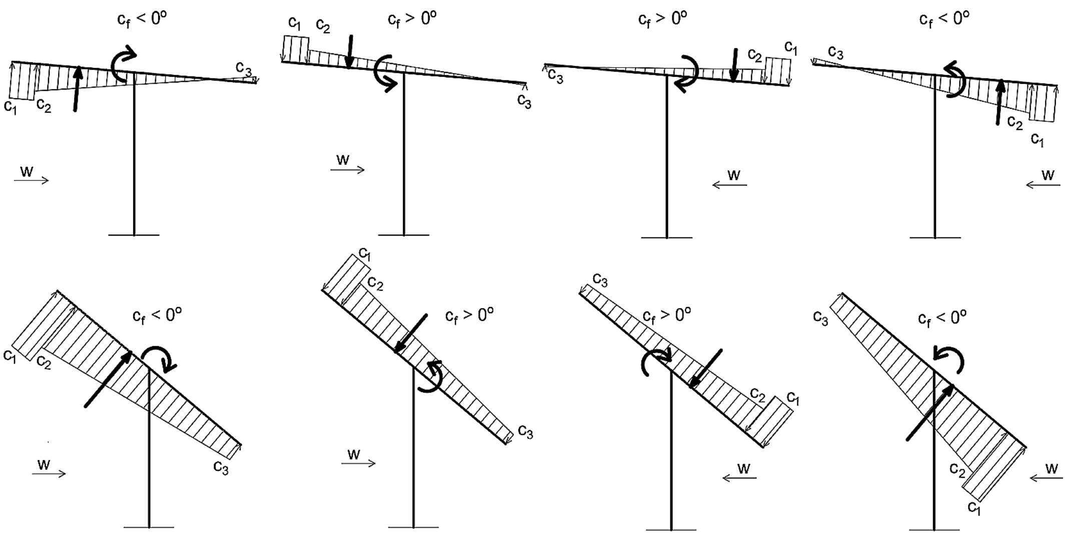

Figure 7. Comparison of loads for inclinations of 5° and 40°. Wind speed 22 m/s

The displacements at the top of the column also exceeded not only the code values (1/150 of the column height) but also the limits permitted by the device manufacturer (30 mm for technological reasons). This may potentially lead to damage to individual panels. A comparison of the column displacements determined using various computational models is shown in Figure 8.

Based on the performed computer simulations, very low natural frequencies of the structure were also identified. The normal modes are presented in Figure 9 and in Table 3. Verification calculations carried out in accordance with [20] demonstrated that the analyzed structure is susceptible to torsional galloping. This case occurs both during the installation phase and after the installation of all required components. It should be noted that performed assessment was primarily focused on compliance with the requirements of current European standards. A more comprehensive dynamic analysis would enable a more thorough understanding of the structural behavior and response.

Structural strengthening possibilities

Based on the analyses performed, it was concluded that, in order to ensure the

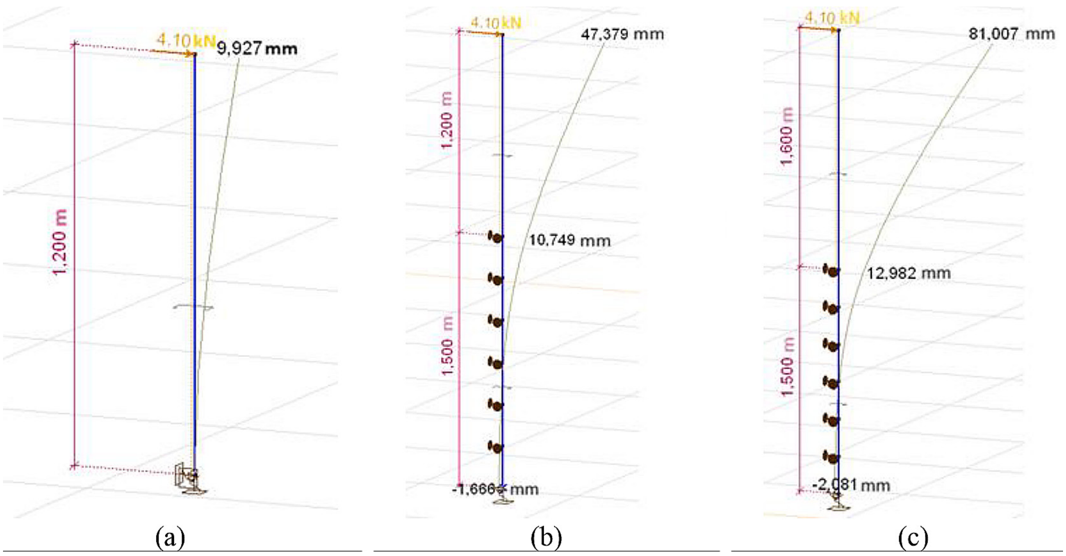

Figure 8. Comparison of horizontal displacement values of the columns depending on the modelling approach: a) model applied in the project, b) model with soil flexibility considered, c) model with soil flexibility considered and with the actual value of the load-application eccentricity

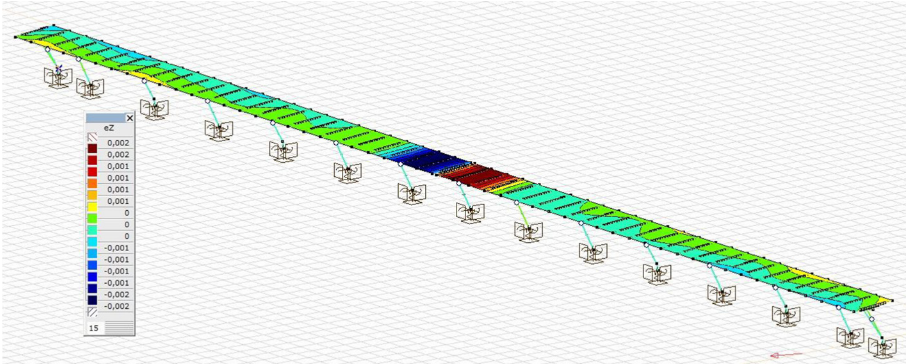

(a)

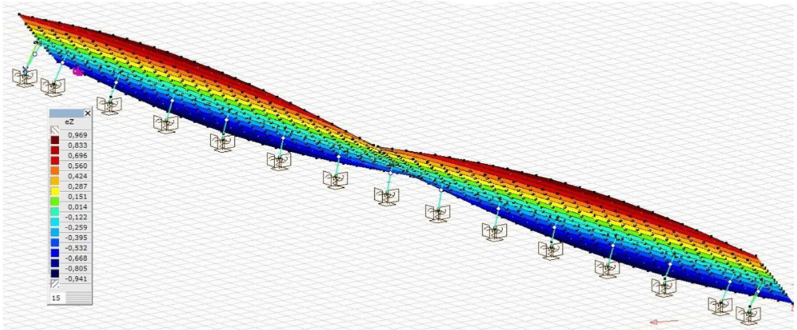

(b)

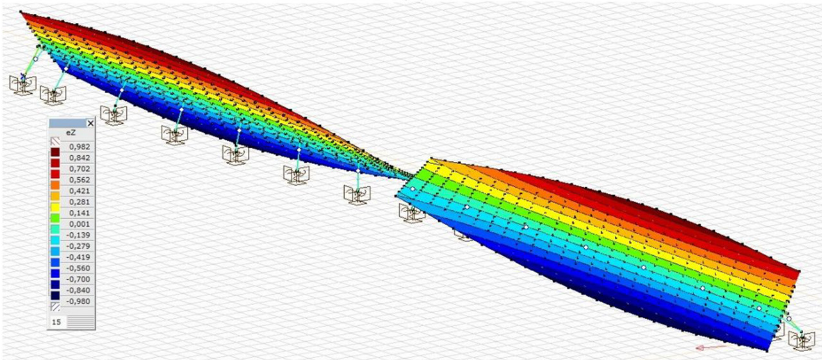

(c)

Figure 9. Normal modes: a) mode 1 – 2.35 Hz b) mode 2 – 3.09 Hz c) mode 3 – 3.27Hz. Vertical displacements in [mm] (e_z) are presented

Table 3. Selected results – verification of torsional galloping condition acc. [19]. v_{cg} – acc. to equation (E.18) of [19]. Applied parameters: S_c = 110.5 (Scruton number), a_g = 10 (galloping instability factor, value unknown case), b = 185mm (structural width, conservatively, natural frequency value according to FEM, δ_s =0,05 (logarithmic decrement of damping for steel building and bridges). All notations acc. to [19], annex E and annex F

Normal mode	Wind speed at which torsional galloping begins [19]	Mean wind velocity acc. [19]	Condition	Comments
2	v_{cg}=12.66 m/s	v_m=14.8 m/s	v_{cg} > 1.25 v_m	Condition not satisfied
3	v_{cg}=13.37 m/s	V_m=14.8 m/s	v_{cg} > 1.25 v_m	Condition not satisfied

proper structural behavior, repair works are recommended. The reduction of horizontal displacements and purlin rotation, as well as the increase of natural vibration frequencies, were identified as key measures. It was proposed to introduce an additional 4 dampers in each row, spaced at 10.2 m from the end of each structure. Such a solution made it possible to eliminate the torsional rotation of the purlin and satisfy the required ultimate limit state criteria. Due to the difficult soil conditions, the displacements of the columns constituted a more significant challenge. Several variants were considered, including, among others, the construction of additional

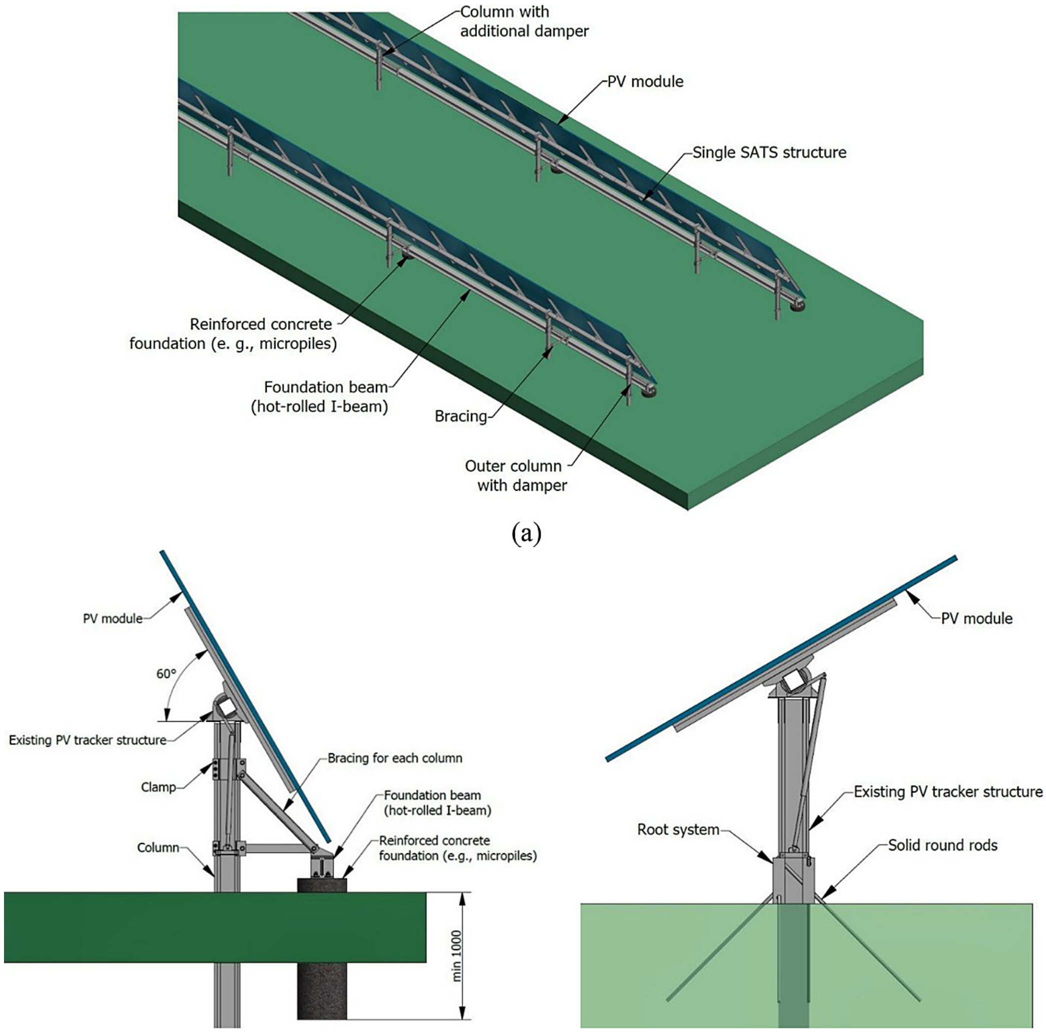

Figure 10. Structural strengthening possibilities: a) & b) – additional foundations and additional dampers, c) steel-root system

Table 4. Comparison of ULS and SLS conditions before and after strengthening

Element	Condition	Existing structure	Strengthened structure "A" (Figure 10b)	Strengthened structure "B" (Figure 10c)
SHS purlin	$\frac{\tau_{Ed}}{f_y/\sqrt{3}\gamma_{M0}}$	144%	82%	82%
C-section column	$\frac{M_{Ed}}{\chi_{LT}W_y f_y/\gamma_{M0}}$	130%	80%	117%
SHS purlin	Purlin rotation angle	36º	6,5º	8º
C-section column (support model)	Horizontal displacement	25 mm	17 mm	20 mm
C-section column (soil-flexibility model)	Horizontal displacement	81 mm	17 mm	44 mm
Structure	Natural frequency	3.09 Hz*	5.39–5.59 Hz	2.66– 4.46 Hz

Note: Loads acc. to [20]. * - minimum values (torsional galloping) for the fixed-support model, **minimum values (torsional galloping) for the fixed support and spring support model, respectively. Values complying with the standard requirements are underlined with single line, values complying with the manufacturer's requirements are underlined with a double line foundations and bracings connecting the new foundations to the columns. Introduction of new additional dampers, bracings and foundations would reduce the torsion of the purlin to up to 6.5°. At the same time horizontal displacements of columns would still exceed the limits recommended by the standards. However, such situation may be considered acceptable due to technological reasons. For the considered solution, all other requirements of the relevant standards are satisfied. Moreover, the natural frequency reaches 5.39 Hz, which makes torsional galloping unlikely. As an alternative, the execution of cement injections around individual columns or the use of a steel-root system was considered. Experimental tests carried out by the contractor demonstrated that steel-root system reduces horizontal displacements by approximately 50%. A combination of steel-roots, dampers and selected bracings also provides satisfactory results in terms of the structural response. Examples of possible strengthening solutions are presented in Figure 10. In the strengthening works, it was also proposed to divide the field into zones with higher and lower wind loads in accordance with standard (Table 4) [6].

CONCLUSIONS

In the article, a case of failure of a new innovative structure of a single-axis support structure for photovoltaic panels was discussed. Within the scope of the conducted work, design errors (incorrect loading schemes) and excessive simplifications in modelling (omission of eccentricities, omission of panel segments, assumed fixed supports, lack of natural frequency analysis) were identified. The safety level of the structure was further reduced by limiting the load values (consideration of the return period, the assumed consequence class). The complex soil conditions and the incomplete state of the structure at the time of the occurrence of relatively strong wind were also significant factors.

Carried out analysis indicated that the requirements of current standards are not satisfied for the considered structure. Ultimate limit state conditions for purlins and columns were significantly exceeded by 30 to 44%. Serviceability limit states were also beyond the allowable limits both for torsion of the purlin and for the displacements of the column (by 170%). Moreover the natural frequency of the structures was too low and as a result torsional galloping was possible. Proposed strengthening methods enabled compliance with the requirements specified in the standards. Introduction of additional bracings, dampers and foundations ensured compliance with most of the limit states. After strengthening, minor exceedance may occur only in the case of column displacements. However, these are acceptable due to technological reasons.

Based on the analyses carried out, conclusions can be drawn that may help to prevent similar failures in the future. In the case of innovative and atypical structures for which there is limited experience regarding their structural behavior, particular caution is required. Due to the critical nature of wind load, it should be thoroughly analyzed. For structures intended for mass production, carrying out wind tunnel tests is strongly expected. Despite the apparent simplicity of the structure, appropriate computational models should be as accurate as possible and should represent the actual structural behavior without unnecessary simplifications. The assumptions adopted for the foundation conditions should be verified in relation to the actual soil conditions present at the construction site. In every case, it is absolutely necessary to perform an analysis of the natural vibration frequencies. When designing utility-scale photovoltaic farms, the relatively low cost of the steel structure compared to the total investment cost must be considered. Above all, the severe economic consequences resulting from delays in project completion, structural failure, or temporary shutdown should be taken into account.

REFERENCES

1. Kumba K., Upender P., Buduma P., Sarkar M., Simon S.P., Gundu V. Solar tracking systems: Advancements, challenges, and future directions: A review, Energy Rep. 2024; 12: 3566–3583. https://doi.org/10.1016/j.egyr.2024.09.038
2. Kołat K., Maślak M., Pazdanowski M., Zajdel P. Mounting of photovoltaic panels supporting structure on transverse frames of a steel hall, Econ. Environ. 2025; 93: 1–15. https://doi.org/10.34659/eis.2025.93.2.1093
3. Kazem H.A., Chaichan M.T., Al-Waeli A.H.A., Sopian K. Recent advancements in solar photovoltaic tracking systems: An in-depth review of technologies, performance metrics, and future trends. Sol. Energy 2024; 282. https://doi.org/10.1016/j.

solener.2024.112946
4. Lewandoski C.F., Santos R.F., Man Kit Sio J.P., de Almeida M., Ikpehai A. The Advantages of Solar Tracker, Int. J. of Environ. Resil. Res. Sci. 2021; 3: 31–46. https://doi.org/10.48075/ijerrs.v3i1.26451
5. Koekemoer J.H., Bredell J.R., Venter G., Reinecke J. Field measurements of wind load effects in a photovoltaic single-axis tracker mounting rail. J. of Wind Eng. Ind. Aerodyn. 2024; 253. https://doi.org/10.1016/j.jweia.2024.105876
6. ASCE 7-22, Standard 7: Minimum design loads and associated criteria for buildings and other structures, American Society of Civil Engineering. 2022.
7. Debnath K., Barman J., Hsieh C.-C., Huang C.-Y., Juang R.-C., Chiu C.-W., Kuo C.-F.J. Wind pressure characterization on ground-mounted solar PV systems: A combined experimental and numerical study. Case Stud. Therm. Eng. 2025; 73. https://doi.org/10.1016/j.csite.2025.106501
8. Rohr C., Bourke P.A., Banks D. Torsional Instability of Single-Axis Solar Tracking Systems, In: Proc. Int. Conf. Wind Eng., Brazil, Porto-Alegre, 2015.
9. Cárdenas-Rondón J.A., Carbajosa C., Marín-Coca S., Martínez-Cava A. Parametric analysis of self-excited aeroelastic instability of an isolated single-axis two-dimensional flat solar tracker. Results Eng. 2024; 24. https://doi.org/10.1016/j.rineng.2024.103539
10. Chen T., Zhang H., Zhang X., Wang F., Li Y., Zhao Q., Ge Y. Experimental study on wind-induced vibration of single-axis solar tracker. Appl. Sci. 2026; 16: 4843. https://doi.org/10.3390/app16104843
11. Opie B., Avci O., Gutta J.B., Quaranta J.D., Taylor S. A brief review of solar panel installations on former mine lands: technical challenges and uncertainties for tracking and foundation systems. Sol. Energy 2025; 300: 113858. https://doi.org/10.1016/j.solener.2025.113858
12. Valentín D., Valero C., Egusquiza M., Presas A. Failure investigation of a solar tracker due to wind-induced torsional galloping, Eng. Fail. Anal. 2022; 135. https://doi.org/10.1016/j.engfailanal.2022.106137
13. Cárdenas-Rondón J.A., Ogueta-Gutiérrez M., Franchini S., Manzanares-Bercial R. Stability analysis of two-dimensional flat solar trackers using aerodynamic derivatives at different heights above ground. J. of Wind Eng. and Ind. Aerodyn.2023; 243. https://doi.org/10.1016/j.jweia.2023.105606
14. Zhang X., Ma W., Li H., Shao Q., Kang X. Experimental investigation of the torsional aeroelastic instability of single-axis solar tracers. Int. J. of Struct. Stab. and Dyn. 2024; 24(1): 2450007. https://doi.org/10.1142/S021945542450007X
15. Kotala B., Szojda L., Failure of support structure of photovoltaic panels due to design errors. In: Proc. Int. Conf. on Struct. Failures, Szczecin, 2024; 543–554.
16. Błaż J., Olczyk N., Failure of the ground-mounting structures at a photovoltaic farm. In: Proc. Int. Conf. on Struct. Failures, Szczecin, 2024; 505–512.
17. Tylek I., Kuchta K., Rawska-Skotniczny A. Human errors in the design and execution of steel structures – a case study. Struct. Eng. Intern. 2017; 27: 370–379. https://doi.org/10.2749/101686617X14881937385287
18. EN 1990, Eurocode 0: Basis of structural and geotechnical design, European Committee for Standardization, Brussels, Belgium, 2023.
19. EN 1991-1-4, Eurocode 1: Actions on structures - Part 1-4: General actions - Wind actions, European Committee for Standardization, Brussels, Belgium, 2005.
20. Ossatures E.T., Acier E.N. Recom. Cnc2M En 1991-1-4 Aux Charpentes, (2017).
21. Inter-CAD, Axis VM X8, (2025).
22. PN-77/B-02011, Loads in static calculations. Wind loads (in Polish), 1977; 41.
23. Gwizdała K., Fundamenty palowe. Technologie i obliczenia, Wydawnictwo Naukowe PWN, Warszawa, 2011.
24. EN 1993-1-1, Eurocode 3: Design of steel structures - Part 1-1: General rules and rules for buildings, European Committee for Standardization, Brussels, Belgium, 2022.
25. EN 1993-1-3, Eurocode 3: Design of steel structures - Part 1-3: General rules – Cold-formed members and sheeting, European Committee for Standardization, Brussels, Belgium, 2024.
26. Zhao L., Maynadier A., Nelias D., Stiffness and fracture analysis of photovoltaic grade silicon plates. Int. J. Solids and Struct. 2016; 97–98: 355–369. https://doi.org/10.1016/j.ijsolstr.2016.07.013